

How Does Unfaithful Reasoning Emerge from Autoregressive Training? A Study of Synthetic Experiments

Fuxin Wang*, Amr Alazali, Yiqiao Zhong*

University of Wisconsin-Madison, Madison, WI, USA

Abstract

Chain-of-thought (CoT) reasoning generated by large language models (LLMs) is often unfaithful: intermediate steps can be logically inconsistent or fail to reflect the causal relationship leading to the final answer. Despite extensive empirical observations, a fundamental understanding of CoT is lacking—what constitutes faithful CoT reasoning, and how unfaithfulness emerges from autoregressive training. We study these questions using well-controlled synthetic experiments, training small transformers on noisy data to solve modular arithmetic expressions step by step, a task we term *Arithmetic Expression Reasoning*. We find that models can learn faithful reasoning that causally follows the underlying arithmetic rules, but only when the training noise is below a critical threshold, a phenomenon attributable to simplicity bias. At higher noise levels, training dynamics exhibit a transition from faithful stepwise reasoning to unfaithful skip-step reasoning via an intermediate mixed mode characterized by a transient increase in prediction entropy. Mechanistic analysis reveals that models learn to encode internal uncertainty by resolving inconsistent reasoning steps, which suggests the emergence of implicit self-verification from autoregressive training. Code is available².

1 Introduction

Large language models (LLMs) have recently achieved remarkable performance on reasoning tasks. Much of this success is attributed to chain-of-thought (CoT) reasoning (Wei et al., 2022b), in which models generate intermediate steps before producing a final answer. Such behavior can be encouraged by training on data with explicit reasoning traces (Lightman et al., 2023), which promotes learning simpler, compositional reasoning steps.

However, the mechanism of CoT reasoning remains largely opaque, and it is unclear whether and when LLMs truly acquire the rules governing the reasoning traces. Despite strong benchmark performance, LLMs are known to have stability issues: evaluation can be fragile under minor benchmark perturbation or data contamination (Alzahrani et al., 2024; Gulati et al., 2024; Hosseini et al., 2024). Moreover, CoT reasoning can be superfluous: LLMs sometimes generate reasoning steps as *post-hoc explanations* for answers they already know, or even fabricate plausible-looking reasoning when prompts steer them toward incorrect solutions (Turpin et al., 2023; Lanham et al., 2023; Barez et al., 2025). The ambiguity has drawn criticisms, as Shojaee et al. (2025) argues that reasoning LLMs create “illusion of thinking”. More broadly, the lack of a principled understanding of CoT reasoning has far-reaching implications for AI safety and alignment (Betley et al., 2025).

Can faithful CoT reasoning be clearly defined? Unfaithful reasoning in LLMs has been widely documented. For instance, Wei et al. (2022b); Bao et al. (2024, 2025) show that models may produce incorrect reasoning alongside correct solutions, or correct reasoning with incorrect solutions. Turpin et al. (2023) find that generated reasoning can depend on spurious features such as prompt cues or the ordering of multiple-choice options. However, there is still no consensus on what constitutes faithful reasoning.

¹Correspondence to: fwang297@wisc.edu, yiqiao.zhong@wisc.edu

²https://github.com/jwtr297/Arithmetic_Expression_Reasoning

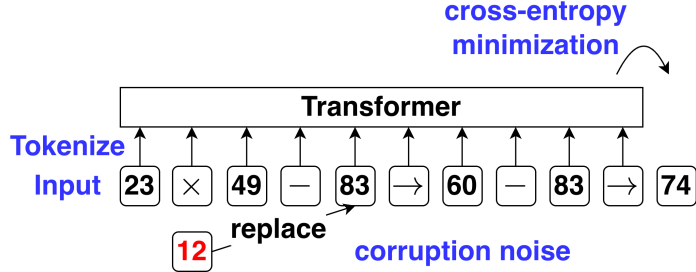


Figure 1: Illustration of our Arithmetic Expression Reasoning (AER) task for CoT reasoning. An input sequence of the format (1) is sampled and tokenized. Then a small transformer is trained from scratch on such data in the standard autoregressive fashion.

Existing approaches for assessing CoT faithfulness fall into two categories. (i) Consistency checking, which examines whether the reasoning steps are logically consistent with the final answer (Lyu et al., 2023). (ii) Intervention on reasoning steps, which tests whether altering the reasoning steps, such as rephrasing or injecting errors, changes the final solution (Turpin et al., 2023; Lanham et al., 2023). These approaches target two key pitfalls of CoT reasoning: mimicking reasoning traces does not guarantee logical consistency, and the sequential structure of a reasoning trace does not imply a causal relationship. Motivated by these empirical studies, we investigate faithful reasoning from both angles.

Model’s internal uncertainty towards unfaithful reasoning. One surprising aspect of LLMs is their meta-reasoning ability to reflect on their own reasoning traces, detect unfaithful reasoning, and thereby improve accuracy. Self-reflection and self-verification (Shinn et al., 2023; Madaan et al., 2023) externalize a model’s internal uncertainty by inducing generated statements like “I’m not sure”. A fundamental question is: how do models develop such reflective behavior through autoregressive training? Empirical evidence suggests that base models such as GPT-3 already exhibit primitive self-reflection abilities (Weng et al., 2023), but the mechanisms of emergence are poorly understood.

Modeling CoT reasoning via a synthetic task. Our synthetic task abstracts the mathematical reasoning benchmark **GSM8K** (Cobbe et al., 2021), for which LLMs generate a sequence of reasoning tokens (the text preceding `####`) by chaining multiple arithmetic expressions step by step, culminating in a final solution (the integer following `####`).

Prompt. “A candle melts by 2 centimeters every hour that it burns. How many centimeters shorter will a candle be after burning from 1:00 PM to 5:00 PM?”

Answer. “The candle burns for $5 - 1 = \text{<<}5-1=4\text{>>}4$ hours. Thus, the candle will be $2 * 4 = \text{<<}2*4=8\text{>>}8$ centimeters shorter. `####` 8.”

Our synthetic task, termed *Arithmetic Expression Reasoning (AER)* task, preserves the arithmetic structure of each question while stripping away natural language. Formally, the training data consist of sequences formatted as arithmetic expression chains, where each chain follows the format:

$$\underbrace{a \times b - c}_{e_1: \text{prompt}} \rightarrow \underbrace{d - c}_{e_2: \text{reasoning}} \rightarrow \underbrace{o}_{e_3: \text{solution}}. \quad (1)$$

Figure 1 shows one training example, which is tokenized as an input sequence to the model for next-token prediction training. In this example, we draw a, b, c uniformly from $\mathcal{V}_N := \{0, 1, 2, \dots, N-1\}$ where $N = 97$ is a fixed prime number, and then we determine d and o based on modulus N arithmetic. Then, we introduce “corruption noise” by randomly selecting a, b with probability ε_1 and d with probability ε_2 , and then replacing it with a uniform random number in \mathcal{V}_N . Conceptually, the noise represents random corruption errors in large corpora and ambiguity of natural languages in describing mathematical objects. In this paper, we focus on autoregressive training (i.e., next-token prediction), which is a standard paradigm for pretraining and supervised finetuning.

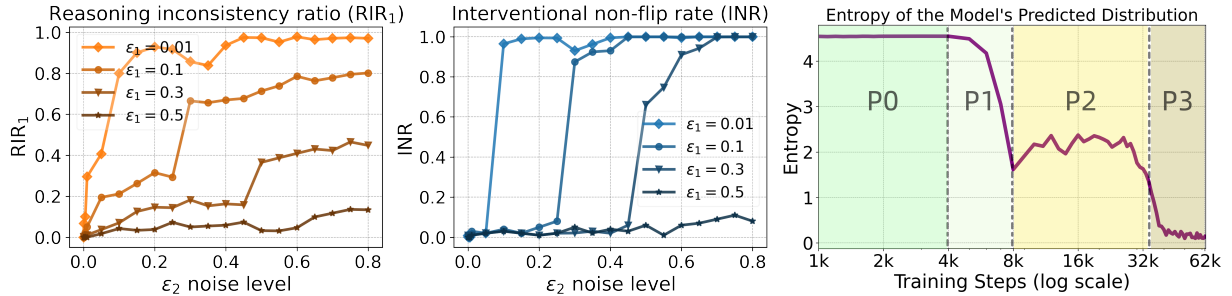


Figure 2: Training small transformers for the AER task. **Left/Middle: evaluating CoT reasoning under two faithfulness definitions.** We train multiple transformers separately on datasets of varying noise levels (ε_1 : prompt noise, ε_2 : reasoning noise). Both unfaithfulness metrics are small at low noise (faithful) until critical thresholds of ε_2 , beyond which unfaithfulness sharply increases—orange curves show generated reasoning chains become less consistent, and blue curves show interventions on reasoning barely change generated solutions. **Right: Prediction entropy across training.** The model experiences four phases: format following (P0), stepwise reasoning (P1), mixed reasoning (P2), and skip-step reasoning (P3). Its prediction uncertainty temporarily increases in P2 as it resolves conflicting information in the reasoning chain, which suggests implicit self-verification behavior.

Our AER task provides a natural and minimal (single reasoning step) compositional structure for CoT reasoning. Compared with prior literature on synthetic tasks, AER is akin to modular arithmetic in grokking (Power et al., 2022), but differs in its focus on the *entire reasoning chain* (both ε_2 and ε_3) rather than solely on the final output. This design opens the door to analyzing reasoning composition.

Main contributions.

1. *A minimal testbed and formal definitions.* We introduce a synthetic task AER and formalize two faithfulness notions: mathematical consistency and counterfactual intervention on reasoning steps.
2. *A faithfulness threshold from simplicity bias.* We find that reasoning faithfulness is possible only when training noise is below a critical threshold, a phenomenon explained by algorithmic simplicity bias.
3. *Three reasoning modes and emergent self-verification.* Under moderate noise, training dynamics exhibit three distinct reasoning modes, with a transition from faithful stepwise reasoning to unfaithful skip-step reasoning through an intermediate mixed mode marked by a transient rise in prediction entropy, indicating emergent implicit self-verification.

2 Setup and Definitions

We will train small transformers to solve the AER task. Following the task setup in the grokking paper (Power et al., 2022), we fix the modulus to be a prime number $N = 97$ for most experiments in the paper. Our input sequences are strings consisting of integers from $\mathcal{V}_N = \{0, 1, \dots, N - 1\}$, operators $\{+, -, \times\}$, and the deduction sign $\{\rightarrow\}$ of the format (1). The vocabulary is $\{0, 1, \dots, N - 1, +, -, \times, \rightarrow\}$, with $N + 4$ tokens in total.

By default, we use standard transformer architecture with 3 layers, 2 heads, 128 embedding dimensions, and rotary positional embedding (RoPE) (Su et al., 2024). The models are trained with AdamW optimizer (Loshchilov and Hutter, 2019) with learning rate 0.001, weight decay 0.01, batch size 512, using the standard autoregressive loss. See Section A for experiment details. All experiments are trained with an A30 GPU. We also consider different variants of experiments where we alter the modulus N , the model size, and the data format, and training sample size. The results are largely the same, which can be found in Section B.

2.1 Data Generation

Let us describe the generation of one training example. First, we generate a noiseless chain by concatenating the components $e_1^0, \rightarrow, e_2^0, \rightarrow, e_3$ following the rules below: e_1^0 contains $a, \text{op}_1, b, \text{op}_2, c$ where a, b, c are uniform integers from \mathcal{V}_N , op_1 is fixed as \times , and op_2 is uniformly samples from $\{+, -\}$; e_2^0 and $e_3 \in \mathcal{V}_N$ are an expression and an integer respectively, by evaluating e_1^0 under modulus N .

Next, for given noise levels $\varepsilon_1, \varepsilon_2 \in [0, 1]$, we inject corruption noise into the expressions as follows: (i) in e_1^0 we select either a or b with equal probability and, with probability ε_1 , replace the selected variable by a uniformly random integer in \mathcal{V}_N , obtaining a new expression denoted by e_1 ; (ii) with probability ε_2 , we replace d in e_2^0 by an independent uniformly random integer in \mathcal{V}_N , obtaining a new expression denoted by e_2 . As an input sequence to the transformer, the resulting chain $e_1 \rightarrow e_2 \rightarrow e_3$ consists of 11 tokens. Note that $e_1 = e_1^0$ with probability $1 - \varepsilon_1$ and $e_2 = e_2^0$ with probability $1 - \varepsilon_2$, so a fraction of training examples contains corruption noise.

Training distribution. Let $\mathcal{E}_1, \mathcal{E}_2, \mathcal{E}_3$ be the space of all possible expressions for e_1, e_2, e_3 respectively. Thus, the training distribution \mathcal{P} is the joint distribution of (e_1, e_2, e_3) over $\mathcal{E}_1 \times \mathcal{E}_2 \times \mathcal{E}_3$ as described in the data generation. The total number of training examples is 2,000,000.

Arithmetic rule as composition. Let $f_1 : \mathcal{E}_1 \rightarrow \mathcal{E}_2$ be the correct deduction and $f_2 : \mathcal{E}_2 \rightarrow \mathcal{V}_N$ be the correct solution. For example, if $e_1 = 2 \times 9 - 19$, $e_2 = 18 - 19$, and $e_3 = 96$, then $f_1(e_1) = e_2$ and $f_2(e_2) = e_3$. CoT reasoning explicitly expresses the arithmetic rule as the composition $f_2 \circ f_1$, denoted as f . The goal is to learn the reasoning chain: given $e_1 \in \mathcal{E}_1$, the model ideally generates

$$e_1 \rightarrow f_1(e_1) \rightarrow \underbrace{f_2(f_1(e_1))}_f. \quad (2)$$

We say that the chain $e_1 \rightarrow e_2 \rightarrow e_3$ is consistent if $e_2 = f_1(e_1)$, $e_3 = f_2(f_1(e_1))$, i.e., satisfying the arithmetic rule as stated above. We write a reasoning chain equivalently $e_1 \rightarrow e_2 \rightarrow e_3$ as a tuple (e_1, e_2, e_3) .

2.2 Two Definitions of Faithful Reasoning

A transformer is a probabilistic model p that gives a probability distribution given a context. Specifically, the conditional probabilities $p(e_2|e_1)$ and $p(e_3|e_1, e_2)$ characterize the model's behavior. Let \mathcal{F}_1 be the function space that maps from \mathcal{E}_1 to \mathcal{E}_2 , and \mathcal{F}_2 be the function space that maps from $\mathcal{E}_1 \times \mathcal{E}_2$ to \mathcal{V}_N . We define two random functions \hat{f}_1, \hat{f}_2 , respectively, as \mathcal{F}_1 -valued and \mathcal{F}_2 -valued random elements satisfying, for all e_1, e_2, e_3 ,

$$\begin{aligned} \mathbb{P}(\hat{f}_1(e_1) = e_2) &= p(e_2|e_1), \\ \mathbb{P}(\hat{f}_2(e_1, e_2) = e_3) &= p(e_3|e_1, e_2). \end{aligned}$$

In reality, due to multiple factors (e.g., noise, underfitting, overfitting), we expect \hat{f}_1, \hat{f}_2 to deviate from f_1, f_2 with positive probabilities, i.e., not accurately learning the (groundtruth) arithmetic rules of f_1 and f_2 .

Consistency-based faithfulness. For a test prompt e_1 , we generate a chain (e_1, e'_2, e'_3) from a given sampling scheme (e.g., greedy decoding or sampling under a certain temperature). A common way of characterizing the reasoning behavior is to compare (e_1, e'_2, e'_3) with the consistent groundtruth chain (e_1, e_2, e_3) (Table 1). We say the CoT reasoning is faithful if $e_2 = e'_2$ and $e_3 = e'_3$ for every prompt e_1 .

This definition is an observational notion of faithfulness without causal dependence. While conceptually simple, it suffers from two drawbacks: (i) The set of consistent chains has cardinality $|\mathcal{E}_1|$, which is a small fraction of the set of all possible chains with cardinality $|\mathcal{E}_1| \times |\mathcal{E}_2| \times |\mathcal{E}_3|$. Thus, we have no out-of-distribution robustness guarantees. (ii) Even when a model generates a consistent chain, we are unable to distinguish genuine step-by-step reasoning from post hoc explanation, where the latter lacks expected causal links.

Table 1: **Consistency-based reasoning categorization.** Given a test instance e_1 , compare the model chain (e_1, e'_2, e'_3) with the ground-truth chain (e_1, e_2, e_3) . Here e'_2 is the reasoning step and e'_3 is the solution; R = reasoning, S = solution.

Type	Consistency check	Outcome
Faithful	$e'_2 = e_2, e'_3 = e_3$	R correct; S correct
	$e'_2 \neq e_2, e'_3 = e_3$	R incorrect; S correct
Unfaithful	$e'_2 = e_2, e'_3 \neq e_3$	R correct; S incorrect
	$e'_2 \neq e_2, e'_3 \neq e_3$	R incorrect; S incorrect

Intervention-based faithfulness. We provide a stronger faithfulness definition by considering counterfactuals of e_2 so that e_1 and e_2 are not necessarily consistent, especially in low-noise settings. This definition requires intervening on the reasoning e_2 and observing the resulting change in solution e_3 —in particular, if e_1 and e_2 are not consistent, how much predicting e_3 depends on e_1 and e_2 . The following definition characterizes two extreme modes.

Definition 2.1. (i) **(Perfect) stepwise reasoning:** We say that a model’s CoT reasoning follows (perfect) stepwise reasoning if the following holds with probability 1: $\hat{f}_2(e_1, e_2) = f_2(e_2)$ for all $e_1 \in \mathcal{E}_1, e_2 \in \mathcal{E}_2$. (ii) **(Perfect) skip-step reasoning:** We say that a model’s CoT reasoning follows (perfect) skip-step reasoning if the following holds with probability 1: $\hat{f}_2(e_1, e_2) = f(e_1)$ for all $e_1 \in \mathcal{E}_1, e_2 \in \mathcal{E}_2$.

Perfect step-by-step reasoning implies that \hat{f}_2 depends solely on the reasoning expression e_2 regardless of e_1 . Similarly, perfect skip-step reasoning implies that \hat{f}_2 only depends e_1 and ignores the reasoning expression e_2 . Under this definition, a model’s CoT reasoning is perfectly faithful if it follows perfect stepwise reasoning and $\hat{f}_1(e_1) = f_1(e_1)$ for all $e_1 \in \mathcal{E}_1$ with probability 1. Clearly, this intervention-based faithfulness implies consistency-based faithfulness.

2.3 Metrics

During training, we evaluate the models using a suite of metrics every 1,000 training steps on 1,000 held-out test examples. We denote the generated reasoning chains by (e'_2, e'_3) given e_1 under a specified decoding scheme.

Consistency-based metrics. We calculate the proportions of the four categories from Table 1 by sampling $n = 1,000$ test prompts $(e_{i,1})_{i \leq n}$ following the training distribution and use the model to generate $(e'_{i,2}, e'_{i,3})$ under a fixed the temperature 1. We mainly consider two metrics of *reasoning inconsistency ratio (RIR)*:

$$\text{RIR}_1 := \frac{\sum_{i \leq n} \mathbf{1}\{e'_{i,2} \neq e_{i,2}, e_{i,3} = e'_{i,3}\}}{\sum_{i \leq n} \mathbf{1}\{e'_{i,2} \neq e_{i,2}\}} \quad (3)$$

$$\text{RIR}_2 := \frac{\sum_{i \leq n} \mathbf{1}\{e'_{i,2} \neq e_{i,2}, e_{i,3} = e'_{i,3}\}}{\sum_{i \leq n} \mathbf{1}\{e'_{i,3} = e_{i,3}\}}. \quad (4)$$

The two metrics differ in the denominators and are complementary in quantifying unfaithfulness (higher means more unfaithful). Intuitively, RIR_1 measures the proportion of recovering a correct solution e_3 when it generates incorrect reasoning e_2 ; and RIR_2 measures the proportion of incorrect reasoning among solution-correct test samples.

Intervention-based metrics. We will apply interventions to reasoning e_2 and measure how well a model fits into the two categorization in Definition 2.1. We will focus on *uniformly random intervention*, where we replace d in e_2 by a uniform random variable in \mathcal{V}_N , which yields \tilde{e}_2 . For n independent test prompts

$(e_{i,1})_{i \leq n}$, model’s generated reasoning $(e'_{i,2})_{i \leq n}$, and the replaced reasoning $(\tilde{e}_{i,2})_{i \leq n}$, we calculate the two metrics: Interventional distribution sensitivity (IDS) and Interventional non-flip rate (INR):

$$\begin{aligned} \text{IDS} &:= \frac{1}{n} \sum_{i=1}^n D_{\text{KL}}(\hat{f}_2(e_{i,1}, e'_{i,2}), \hat{f}_2(e_{i,1}, \tilde{e}_{i,2})); \\ \text{INR} &:= \frac{1}{n} \sum_{i=1}^n \mathbf{1}\{ \arg \max_{e \in \mathcal{V}_N} p(e|e_{i,1}, e'_{i,2}) = \arg \max_{e \in \mathcal{V}_N} p(e|e_{i,1}, \tilde{e}_{i,2}) \}. \end{aligned}$$

where D_{KL} means KL divergence. A small IDS and a large INR mean weak causal effects of e_2 on e_3 , which are indications of skip-step reasoning. Conversely, a large IDS and a small INR are evidence of stepwise reasoning.

Prediction uncertainty metrics. We measure a model’s uncertainty with prediction entropy: for test prompts $(e_{i,1})_{i \leq n}$ and the model’s generated chains $(e'_{i,2}, e'_{i,3})_{i \leq n}$, we calculate prediction entropy (PE):

$$\text{PE} := \frac{1}{n} \sum_{i=1}^n \sum_{e \in \mathcal{V}_N} -p(e|e_{i,1}, e'_{i,2}) \log p(e|e_{i,1}, e'_{i,2}). \quad (5)$$

3 Main Results

3.1 How Does Noise Induce Unfaithfulness?

We construct training data of varying noise levels ε_1 and ε_2 . In particular, the training data is noiseless when $\varepsilon_1 = \varepsilon_2 = 0$. For each combination of $(\varepsilon_1, \varepsilon_2)$, we train a transformer for 62,500 steps and evaluate the model at the final checkpoint.

Our aim is to investigate factors, particularly noise levels, that impact faithfulness of reasoning. While we anticipate that lower noise levels improve consistency-based faithfulness, it is a priori unclear whether intervention-based faithfulness is possible at all. Consider training a model with noiseless training data ($\varepsilon_1 = \varepsilon_2 = 0$). Observing only consistent chains, the model could theoretically learn the solution $\hat{f}_2(e_1, e_2)$ as $f_1(e_1)$, $f_2(e_2)$, or a mix of the two—all of which would achieve zero loss and perfect consistency-based faithfulness. Yet, only learning $f_2(e_2)$ satisfies intervention-based faithfulness criteria. Thus, we ask the question—*Is intervention-based faithfulness possible at all? If so, what are contributing factors?*

Intervention-based faithfulness is possible below a critical noise level. We find that faithful reasoning is achievable, but only when the noise level is sufficiently small. In Figure 2 (left/middle), we consider prompt noise level $\varepsilon_1 \in \{0.01, 0.1, 0.3, 0.5\}$ and vary the reasoning noise level $\varepsilon_2 \in \{0.001, 0.005, 0.01, 0.05, 0.1, 0.3, 0.5, 0.9\}$. We measure unfaithfulness with two metrics, namely consistency-based RIR₁ and intervention-based INR, and find that both metrics are non-decreasing as the noise level increases.

Moreover, Figure 2 reveals the existence of a critical threshold $\tau_c(\varepsilon_1)$ exists in ε_2 for each ε_1 . Indeed, both unfaithfulness metrics are approximately flat and close to 0 below the threshold $\tau_c(\varepsilon_1)$, and increase dramatically beyond the thresholds. This suggests that competition between e_1 and e_2 as predictive signals for lowering loss largely determines reasoning behavior at the final checkpoint.

Interestingly, both unfaithfulness metrics are close to 0 under the noiseless setting ($\varepsilon_1 = \varepsilon_2 = 0$), indicating that faithful reasoning is achievable when training only on consistent chains. More generally $\varepsilon_1 < \tau_c(\varepsilon_1)$, which means that at low noise, models exhibit inertia: it continues to rely on stepwise reasoning rather than immediately switching to skip-step reasoning for a slightly lower loss. This motivates a study of algorithmic effects beyond noise levels alone.

Faithfulness benefits from simplicity bias (low-complexity preference). We hypothesize that the training algorithm favors learning a simpler rule (stepwise reasoning involving a single operator) over a more complex rule (skip-step reasoning involving two operators) if both mechanisms yield comparable accuracy. This hypothesis is based on Occam’s razor and recent theoretical study of inductive bias in overparametrized

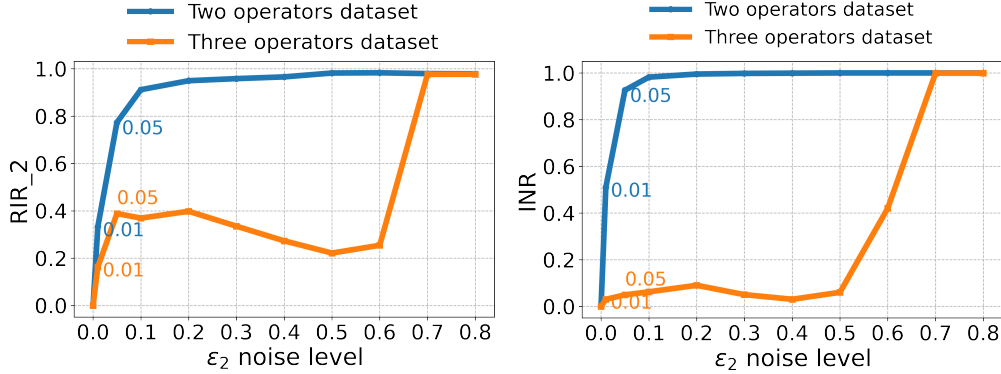


Figure 3: **Larger complexity gap between e_1 and e_2 reduces unfaithfulness.** Fixing $\epsilon_1 = 0.01$, we sweep ϵ_2 and compare training transformers on two-operator prompts e_1 and three-operator prompts. Both metrics indicate that larger difficulty gaps encourage stepwise reasoning and reduce unfaithfulness.

neural networks (Soudry et al., 2018; Montanari and Zhong, 2022; Abbe et al., 2024), where models prefer smooth, low-degree, and low-complexity functions.

To validate this hypothesis, we modify the experiment to increase the complexity gap between the prompt and reasoning: in data generation, we replace $e_1^0 = a \times b - c$ with $(a + b) \times c - d$, and inject noise in e_1 by randomly replacing a , b , or c at noise level ϵ_1 while the noise injection scheme for e_2 remains unchanged; we also changed the modulus to $N = 29$. This modification increases the reasoning complexity of $e_1 \rightarrow e_2$ which evaluates 2 operators in one step. Figure 3 shows that a larger complexity gap between e_1 and e_2 reduces unfaithfulness, and that models tolerate higher reasoning noise before the sharp transition to skip-step reasoning. The results demonstrate that a larger complexity gap between successive steps in the reasoning chain induces a stronger simplicity bias, which creates an algorithmic barrier for the model to develop unfaithful skip-step reasoning.

Finally, we show that the complexity gap between reasoning steps—not the relative positions—forms the algorithmic inductive bias, thereby excluding a confounding factor. Specifically, we swap the positions of the prompt and the reasoning, so that the modified chain becomes $e_2 \rightarrow e_1 \rightarrow e_3$. Section B.1 shows that reasoning faithfulness is determined by complexity, and not by relative positions.

Practical Implication. Low noise in training data and large complexity gaps in reasoning steps are critical to inducing high faithfulness in CoT reasoning.

3.2 Phases of Reasoning Modes Across Training

Phase characterization of reasoning modes. We find that a model’s reasoning mode evolves across training in a single experiment. For illustration, we fix the noise level to be $\epsilon_1 = 0.01, \epsilon_2 = 0.1$ to generate the training data and train the model for 62,500 steps. We are mostly interested in the model’s probability distribution of $\hat{f}_2(e_1, e_2)$ across training. We hypothesize that the model is characterized by the following four phases with respect to training step t . Let (e_1, e_2) follows the same distribution as the training data.

- *Phase 0 (format following):* predicting operator token “+” or “-” and deduction “ \rightarrow ” in correct positions.
- *Phase 1 (stepwise reasoning):* prediction depends mostly on e_2 in the sense of $\hat{f}_2(e_1, e_2) \approx f_2(e_2)$.
- *Phase 2 (mixed reasoning):* Denote the indicator $c(e_1, e_2) = \mathbf{1}\{f(e_1) = f_2(e_2)\}$. Then $\hat{f}_2(e_1, e_2) \approx f_2(e_2)c(e_1, e_2) + U(1 - c(e_1, e_2))$ where U is a uniform random variable in \mathcal{V}_N . That is, prediction is most uncertain (uniform distribution) if e_1 and e_2 are inconsistent, and consistent with both e_1, e_2 otherwise.
- *Phase 3 (skip-step reasoning):* prediction depends mostly on e_1 in the sense of $\hat{f}_2(e_1, e_2) \approx f(e_1)$.

We validate the hypothesized characterization using several evaluation metrics (Figures 4 and 11). (i) **Format score:** we generate the full reasoning traces and solutions given test prompts, and calculate

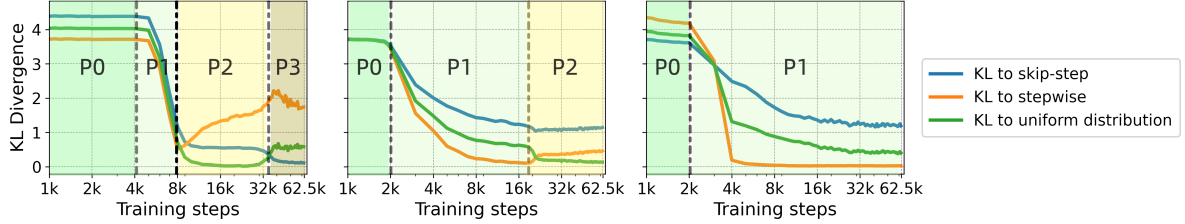


Figure 4: **Training dynamics exhibit distinct phases of reasoning modes.** We conduct three experiments under different noise configurations and evaluate models with three metrics (logarithmic x-axis). **Left:** Noise levels $(\varepsilon_1, \varepsilon_2) = (0.01, 0.1)$. The model exhibits four distinct reasoning phases, validating our proposed phase characterization. **Middle:** $(\varepsilon_1, \varepsilon_2) = (0.1, 0.1)$. The model exhibits only the first three phases, as equal noise levels incentivizes the model to stay in the mixed reasoning mode P2. **Right:** $(\varepsilon_1, \varepsilon_2) = (0.1, 0.01)$. The model exhibits only the first three phases, as lower prompt noise incentivizes stepwise reasoning P1.

the rate of generating operators and deduction tokens at correct positions. (ii) **KL to stepwise**: we calculate the KL divergence between the model’s prediction probability and perfect stepwise reasoning $n^{-1} \sum_{i \leq n} D_{\text{KL}}(\hat{f}_2(e_{i,1}, e'_{i,2}), f_2(e'_{i,2}))$ where $(e_{i,1}, e'_{i,2})_{i \leq n}$ is generated based on $n = 1,000$ test prompts $e_{i,1}$. (iii) **KL to skip-step**: we calculate the KL divergence between the model’s prediction probability and perfect skip-step reasoning $n^{-1} \sum_{i \leq n} D_{\text{KL}}(\hat{f}_2(e_{i,1}, e'_{i,2}), f(e_{i,1}))$ where $(e_{i,1}, e'_{i,2})_{i \leq n}$ is similarly sampled and generated. (iv) **KL to uniform distribution**: we calculate the KL divergence between the model’s prediction distribution and a uniform distribution $n^{-1} \sum_{i \leq n} D_{\text{KL}}(\hat{f}_2(e_{i,1}, e'_{i,2}), U)$ evaluated only on inconsistent chains where $f(e_1) \neq f_2(e_2)$. We note reasoning modes in Phase 1–3 have causal interpretations; see Section B.2 and Figure 10 for further explanations.

Our results support our phase characterization. Figure 11 in Section B.2 shows that the model quickly learns format following in Phase 0. In Figure 4 (left) P1, the orange curve quickly descends to the minimum and is the smallest among the three KL divergence metrics, which indicates the model’s preference for stepwise reasoning in the early phase of training. In P2, the orange curve rises while the blue curve drops to approximately 0. This indicates that the model moves away from stepwise reasoning, and learns to predict a uniform distribution (least informative) for inconsistent chains (e_1, e_2) . In P3, the blue curve further descends to its minimum and is the smallest among the three metrics, which indicates that the model eventually learns skip-step reasoning driven by loss minimization.

We also find that under different noise configurations, models may only reach Phase 1 or Phase 2. Figure 4 (middle) shows that models trained with equal noise levels eventually stay in the mixed reasoning mode, since combining both the prompt and the reasoning expressions yields the smallest loss. Figure 4 (right) shows another experiment with a smaller reasoning noise, which discourages the model to rely on the prompt expression e_1 .

Factors that determine reasoning modes. Based on the above experiments, we hypothesize that two deciding factors of a model’s reasoning mode are data quality (namely noise levels) and compute (namely training steps). We fix $\varepsilon_1 = 0.1$ and let the reasoning noise level ε_2 range from 0.001 to 0.9. For each noise level and evaluation checkpoint during training, we classify the model’s reasoning mode into P1, P2, or P3, based on whichever phase has the smallest KL divergence among the three KL metrics. Figure 9 in Section B.2 shows that more compute and higher prompt noise generally push the model towards skip-step reasoning. As a side result, we also find that the phase boundaries are irregular and vary across different random seeds, suggesting the complexities of the optimization landscape, which echos the unpredictability of emergent phenomena in LLMs (Wei et al., 2022a).

Practical Implication. *Prolonged autoregressive training for CoT reasoning (particularly supervised fine-tuning) may reduce faithfulness by encouraging skip-step reasoning.*

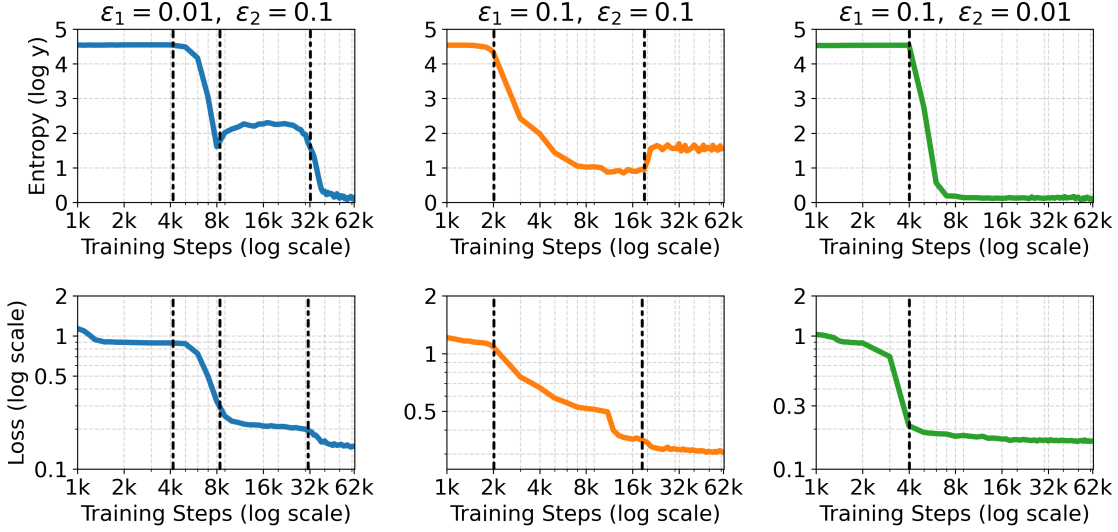


Figure 5: **Prediction entropy shows a temporary ascent despite continuously decreasing training loss.** Models encode reasoning uncertainty in the mixed reasoning mode, which matches most sharp descents of the loss.

3.3 Implicit Self-Verification

Meta-reasoning abilities such as self-reflection and self-verification are intriguing emergent skills from reasoning scaling (Guo et al., 2025). We aim to closely examine mixed reasoning mode and address the following questions—*Does the model learn to encode reasoning uncertainty? If so, what is its internal mechanism?*

Prediction entropy momentarily increases during mixed reasoning mode. We use the prediction entropy (5) to quantify the model’s uncertainty, an approach used in recent empirical papers (Fu et al., 2025; Zhao et al., 2025). In the presence of inconsistent chains (e_1, e_2), our Phase 2 characterization of the mixed reasoning mode suggests that model outputs approach a near-uniform distribution, corresponding to maximal uncertainty. Figure 5 (top) confirms this behavior: under the three noise configurations as in Figure 4, prediction entropy exhibits a clear non-monotonic trend, rising as the model enters the mixed reasoning mode.

Figure 5 (bottom) shows the evolution of the training loss. Unlike prediction entropy, the loss decreases monotonically, as expected. Yet, most sharp drops in loss align closely with transitions between reasoning modes. This correspondence suggests that changes in reasoning behavior and uncertainty are reflected in the geometry of the loss landscape.

A mechanistic analysis reveals uncertainty-encoding features. To probe how the model internally represents uncertainty, we examine the evolution of top-layer hidden states throughout training. The PCA visualization in Figure 6 shows that hidden states encode the distinct reasoning phases, with clear changes in trajectory direction aligned with phase transitions.

Moreover, we examine whether certain coordinates of hidden states encode uncertainty features and the effects of attentions. To this end, we introduce:

Hidden State Contrast (HSC) :=

$$\frac{1}{n} \sum_{i=1}^n \left| \left\| h_{L,e_3}(e_{i,1}^+, e_{i,2}^+) \right\|_\infty - \left\| h_{L,e_3}(e_{i,1}^-, e_{i,2}^-) \right\|_\infty \right|,$$

Attention Contrast (AC) :=

$$\frac{1}{n} \sum_{i=1}^n \left\| h_{L-1,i}^+ W_{QK}^{(L)} (h_{L-1,i}^+)^T - h_{L-1,i}^- W_{QK}^{(L)} (h_{L-1,i}^-)^T \right\|_{\text{op}},$$

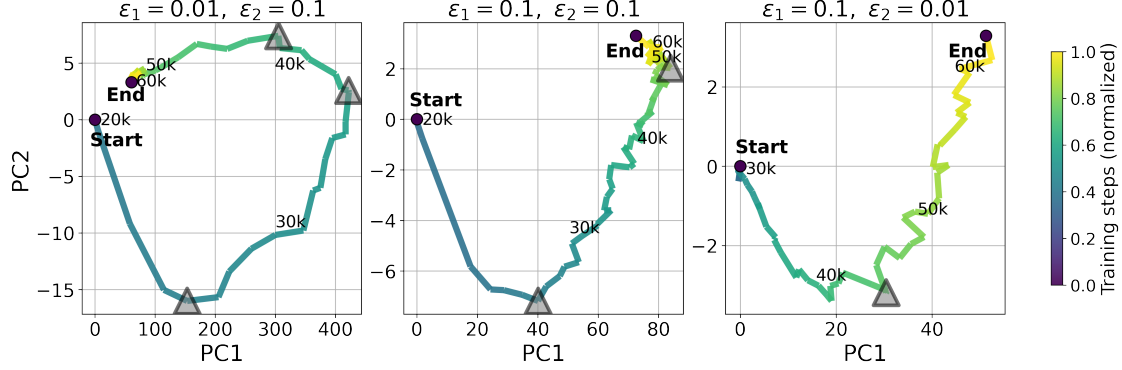


Figure 6: **PCA trajectories of hidden states visualize reasoning phases.** Under three experiment settings, we extract the top-layer hidden states, and project them to the principal subspace. **Left:** Noise levels $(\varepsilon_1, \varepsilon_2) = (0.01, 0.1)$. Triangles mark the changes in movement directions, which correspond to the three phase. **Middle:** Noise levels $(\varepsilon_1, \varepsilon_2) = (0.1, 0.1)$. Phase changes are marked by two triangles. **Right:** Noise levels $(\varepsilon_1, \varepsilon_2) = (0.1, 0.01)$. One triangle marks the only one directional change.

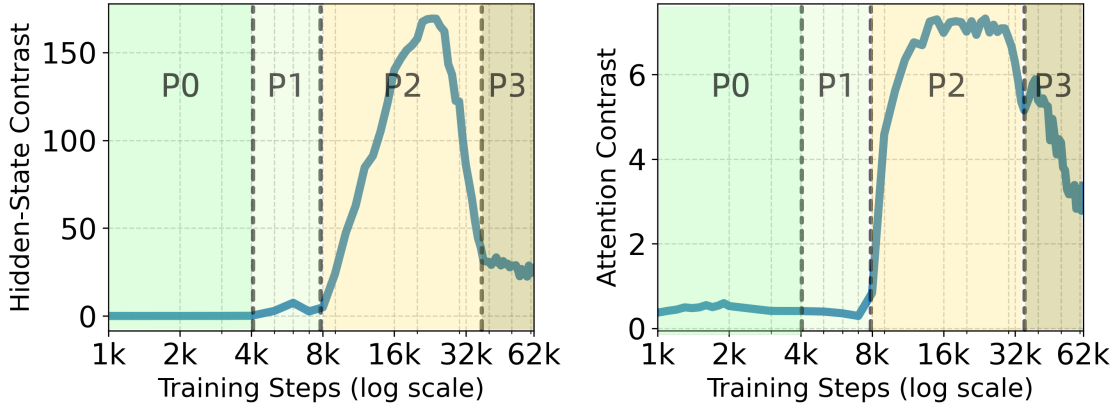


Figure 7: **Emergence of internal uncertainty via mechanistic analysis:** Evolution of HSC and AC at noise levels $\varepsilon_1 = 0.01$ and $\varepsilon_2 = 0.1$. Both metrics experience sharp ascents and subsequent declines, matching phase changes of prediction entropy.

where $\|\cdot\|_{\text{op}}$ denotes the matrix operator norm (Section B.3). Here, we sample consistent (noiseless) chains (e_1^+, e_2^+) as **positive** samples, and inconsistent (noisy) chains (e_1^-, e_2^-) as **negative** samples with noise level $\varepsilon_1 = 0, \varepsilon_2 = 1$ (i.e., e_1 and e_2 always yield different results). We denote by $h_{L, e_3}(e_1^+, e_2^+)$ the post-FFN output vector at the solution e_3 position from the last layer L , and by $h_{L-1, i}^+$ the hidden-state matrix at the penultimate layer $L - 1$ for the i -th positive sample. $h_{L, e_3}(e_1^-, e_2^-)$ and $h_{L-1, i}^-$ are defined analogously. These two quantities measure the degree of differentiation between positive and negative samples, with larger values indicating stronger internal differentiation that functions like consistency checks.

Figure 7 shows both metrics exhibit sharp changes at the same phase thresholds of reasoning modes. This indicating that model internally encodes consistency checks between e_1 and e_2 , resembling a self-verification mechanism that is expressed externally as prediction uncertainty.

Practical Implication. *Reasoning uncertainty is encoded by the model through autoregressive training (including pretraining and supervised finetuning), serving the cornerstone for meta-reasoning abilities such as self-verification.*

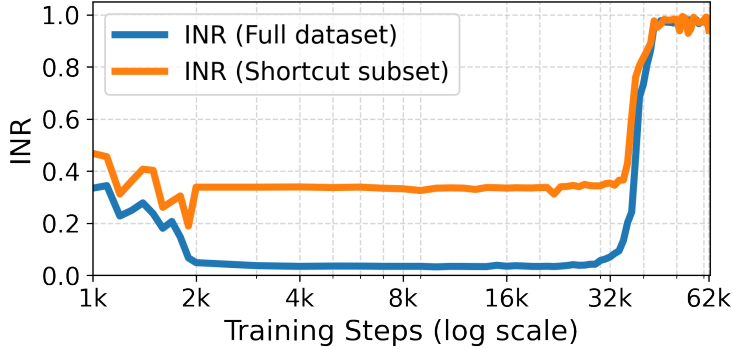


Figure 8: **Training dynamics of intervention-based metrics on the shortcut and full datasets.** INR, as a measure of unfaithfulness, becomes large early, which indicates exploitation of shortcut features undermines reasoning faithfulness.

4 How Shortcut Features Amplify Unfaithfulness

Empirical studies have shown that LLMs are prone to shortcut features that spuriously correlate with solutions (Turpin et al., 2023), which incentivizes models to bypass step-by-step reasoning. For example, adding the cue “A famous professor thinks the solution is option C” to the prompt motivates the model to follow the suggested answer regardless of its correctness, together with unfaithful post-hoc rationalization of this answer. We view instruction cues as shortcut features that can be used to bypass reasoning.

We investigate the effects of shortcut features by modifying our experiment setting. We replace the modulus with a composite number $N = 38$ and sample prompts and reasoning traces in a different format, for example:

$$(a - b) \times c \rightarrow d \times c \rightarrow o,$$

where the first operator in e_1 is uniformly sampled from $\{+, -\}$, and the second operator is \times . As before, all expressions are determined under modulus N .

Shortcut features. We view $\mathbf{1}\{c = 0 \text{ or } c = 2 \text{ or } c = N/2\}$ as the shortcut feature, which has a direct correlation with the solution. Indeed, when $c = 0$ or $c = 2$ or $c = N/2$, there is a high probability that $o = 0$ without deriving the intermediate reasoning step e_2 . To evaluate the impact of shortcut features on reasoning faithfulness, we use two test datasets: (i) full test dataset: $n = 1,000$ test prompts following the training distribution; (ii) shortcut test subset: a subset of 1000 samples selected from an additional test set, where $c \in \{0, 2, N/2\}$ in the prompt expression e_1 .

In Figure 8, we report intervention-based unfaithfulness metrics over training under the noise setting $(\varepsilon_1, \varepsilon_2) = (0.01, 0.1)$. Throughout training, INR is consistently lower on the shortcut test set than on the full test set, indicating a stronger reliance on skip-step reasoning whenever shortcuts are available. We also compute consistency-based metrics such as RIR₁ (Section B.4), which corroborate this behavior from a complementary perspective.

5 Related Work

Training dynamics on synthetic tasks. To understand the learning dynamics of non-reasoning LLMs, well-controlled synthetic tasks have been proposed as proxies for extensive experiments. For example, solving modular arithmetic (e.g., addition, multiplication) requires learning algebraic rules, which exhibits the intriguing grokking phenomenon (Power et al., 2022), where models memorize training data long before abruptly generalizing. For copying task, Elhage et al. (2021); Olsson et al. (2022); Song et al. (2025) identified induction heads as key components for copying arbitrary sequences from context. Through in-context linear regression (Garg et al., 2022; Von Oswald et al., 2023), in-context learning has been shown to behave as a

meta-learning algorithm akin to gradient descent. However, none of these works focus on CoT reasoning or test-time composition. In contrast, our AER task aims to fill this gap.

Faithfulness of CoT reasoning. Prior work offers an empirical account of reasoning faithfulness of pretrained LLMs. It is shown that spurious features and prompt cues shape generated reasoning, suggesting that CoT may function as post-hoc rationalization of answers rather than a causal reasoning process (Turpin et al., 2023; Arcuschin et al., 2025; Chen et al., 2025; Chua and Evans, 2025; Guan et al., 2025). To address this issue, Turpin et al. (2023); Lanham et al. (2023); Bao et al. (2024, 2025) proposed intervention-based metrics to assess the causal relationships within reasoning traces. However, without clean experiment setups targeted at CoT reasoning, existing works lack a principled framework for faithfulness. Moreover, they focus on static models instead of the emergence of unfaithfulness, yet the latter is critical to understanding the causes of unintended reasoning behaviors, with implications for misalignment and AI safety. In contrast, our work studies the learning dynamics using a clean experimental setup.

Self-reflection and uncertainty metrics. LLMs exhibit striking meta-reasoning skills since GPT-3 (Brown et al., 2020; Weng et al., 2023). The abilities of self-reflection and self-verification are further boosted through iterative refinement (Madaan et al., 2023) and post-training (Guo et al., 2025), which significantly reduce inconsistency and unfaithfulness. Recent work has demonstrated the promise of leveraging such metrics to improve LLM reasoning (Fu et al., 2025; Zhao et al., 2025). However, existing empirical advances offer little insight into the underlying mechanism: how these meta-reasoning skills are developed through training, and how the models internally represent such skills. Our work addresses this gap by offering a mechanistic account: models learn to encode consistency checks and internal uncertainty as they resolve inconsistencies in reasoning traces over the course of training.

6 Limitations and Future Work

Our work focuses on autoregressive training which is the standard training paradigm for pretraining and supervised finetuning (SFT). In future work, it would be interesting to investigate reinforcement learning with verifier rewards (RLVR) (Guo et al., 2025) which becomes a standard recipe for enhancing LLM’s reasoning capabilities. We would also be interested in applying our metrics to LLMs beyond our synthetic setting.

Impact Statement

Our work analyzes the fundamental mechanism of CoT reasoning using controlled synthetic experiments. We do not train new models or study practical enhancements that may lead to harmful applications. The main positive impact is to improve scientific understanding of CoT reasoning, particularly the mechanism of unfaithfulness in autoregressive training. Through clear definitions, evaluation metrics, and principled analysis, our results may offer insights to improve the reliability of reasoning capabilities of LLMs. In particular, our findings about models’ internal uncertainty and implicit self-verification offer insights into meta-reasoning skills and may lead to safer finetuning techniques. A potential negative impact is over-generalization of our findings beyond the synthetic task. Our conclusions would require further extensive evaluations across LLMs and tasks before being used in policy making or deployment decisions.

Acknowledgments

Y.Z. is partially supported by NSF-DMS grant 2412052 and by a Coefficient Giving (formerly Open Philanthropy) grant. We also thank Bin Yu for helpful discussions.

References

Emmanuel Abbe, Samy Bengio, Aryo Lotfi, and Kevin Rizk. Generalization on the unseen, logic reasoning and degree curriculum. *Journal of Machine Learning Research*, 25(331):1–58, 2024.

Norah Alzahrani, Hisham Alyahya, Yazeed Alnumay, Sultan Alrashed, Shaykhah Alsubaie, Yousef Almushayqih, Faisal Mirza, Nouf Alotaibi, Nora Al-Twaresh, Areeb Alowisheq, et al. When benchmarks are targets: Revealing the sensitivity of large language model leaderboards. In *Proceedings of the 62nd Annual Meeting of the Association for Computational Linguistics (Volume 1: Long Papers)*, pages 13787–13805, 2024.

Iván Arcuschin, Jett Janiak, Robert Krzyzanowski, Senthooran Rajamanoharan, Neel Nanda, and Arthur Conmy. Chain-of-thought reasoning in the wild is not always faithful. *arXiv preprint arXiv:2503.08679*, 2025.

Guangsheng Bao, Hongbo Zhang, Linyi Yang, Cunxiang Wang, and Yue Zhang. Llms with chain-of-thought are non-causal reasoners. *CoRR*, 2024.

Guangsheng Bao, Hongbo Zhang, Cunxiang Wang, Linyi Yang, and Yue Zhang. How likely do llms with cot mimic human reasoning? In *Proceedings of the 31st International Conference on Computational Linguistics*, pages 7831–7850, 2025.

Fazl Barez, Tung-Yu Wu, Iván Arcuschin, Michael Lan, Vincent Wang, Noah Siegel, Nicolas Collignon, Clement Neo, Isabelle Lee, Alasdair Paren, et al. Chain-of-thought is not explainability. *Preprint, alphaXiv*, page v1, 2025.

Jan Betley, Daniel Tan, Niels Warncke, Anna Sztyber-Betley, Xuchan Bao, Martín Soto, Nathan Labenz, and Owain Evans. Emergent misalignment: Narrow finetuning can produce broadly misaligned llms. *arXiv preprint arXiv:2502.17424*, 2025.

Tom Brown, Benjamin Mann, Nick Ryder, Melanie Subbiah, Jared D Kaplan, Prafulla Dhariwal, Arvind Neelakantan, Pranav Shyam, Girish Sastry, Amanda Askell, et al. Language models are few-shot learners. *Advances in neural information processing systems*, 33:1877–1901, 2020.

Yanda Chen, Joe Benton, Ansh Radhakrishnan, Jonathan Uesato, Carson Denison, John Schulman, Arushi Somani, Peter Hase, Misha Wagner, Fabien Roger, et al. Reasoning models don’t always say what they think. *arXiv preprint arXiv:2505.05410*, 2025.

James Chua and Owain Evans. Are deepseek r1 and other reasoning models more faithful? *arXiv preprint arXiv:2501.08156*, 2025.

Karl Cobbe, Vineet Kosaraju, Mohammad Bavarian, Mark Chen, Heewoo Jun, Lukasz Kaiser, Matthias Plappert, Jerry Tworek, Jacob Hilton, Reiichiro Nakano, et al. Training verifiers to solve math word problems. *arXiv preprint arXiv:2110.14168*, 2021.

Nelson Elhage, Neel Nanda, Catherine Olsson, Tom Henighan, Nicholas Joseph, Ben Mann, Amanda Askell, Yuntao Bai, Anna Chen, Tom Conerly, Nova DasSarma, Dawn Drain, Deep Ganguli, Zac Hatfield-Dodds, Danny Hernandez, Andy Jones, Jackson Kernion, Liane Lovitt, Kamal Ndousse, Dario Amodei, Tom Brown, Jack Clark, Jared Kaplan, Sam McCandlish, and Chris Olah. A mathematical framework for transformer circuits. *Transformer Circuits Thread*, 2021. <https://transformer-circuits.pub/2021/framework/index.html>.

Yichao Fu, Xuewei Wang, Yuandong Tian, and Jiawei Zhao. Deep think with confidence. *arXiv preprint arXiv:2508.15260*, 2025.

Shivam Garg, Dimitris Tsipras, Percy S Liang, and Gregory Valiant. What can transformers learn in-context? a case study of simple function classes. *Advances in Neural Information Processing Systems*, 35:30583–30598, 2022.

Melody Y Guan, Miles Wang, Micah Carroll, Zehao Dou, Annie Y Wei, Marcus Williams, Benjamin Arnav, Joost Huizinga, Ian Kivlichan, Mia Glaese, et al. Monitoring monitorability. *arXiv preprint arXiv:2512.18311*, 2025.

Aryan Gulati, Brando Miranda, Eric Chen, Emily Xia, Kai Fronsdal, Bruno de Moraes Dumont, and Sanmi Koyejo. Putnam-axiom: A functional and static benchmark for measuring higher level mathematical reasoning. In *The 4th Workshop on Mathematical Reasoning and AI at NeurIPS’24*, 2024.

Daya Guo, Dejian Yang, Haowei Zhang, Junxiao Song, Ruoyu Zhang, Runxin Xu, Qihao Zhu, Shirong Ma, Peiyi Wang, Xiao Bi, et al. Deepseek-r1: Incentivizing reasoning capability in llms via reinforcement learning. *arXiv preprint arXiv:2501.12948*, 2025.

Arian Hosseini, Alessandro Sordoni, Daniel Kenji Toyama, Aaron Courville, and Rishabh Agarwal. Not all llm reasoners are created equal. In *The First Workshop on System-2 Reasoning at Scale, NeurIPS'24*, 2024.

Andrej Karpathy. NanoGPT. <https://github.com/karpathy/nanoGPT>, 2022.

Tamera Lanham, Anna Chen, Ansh Radhakrishnan, Benoit Steiner, Carson Denison, Danny Hernandez, Dustin Li, Esin Durmus, Evan Hubinger, Jackson Kernion, et al. Measuring faithfulness in chain-of-thought reasoning. *CoRR*, 2023.

Hunter Lightman, Vineet Kosaraju, Yuri Burda, Harrison Edwards, Bowen Baker, Teddy Lee, Jan Leike, John Schulman, Ilya Sutskever, and Karl Cobbe. Let's verify step by step. In *The Twelfth International Conference on Learning Representations*, 2023.

Ilya Loshchilov and Frank Hutter. Decoupled weight decay regularization. In *International Conference on Learning Representations*, 2019. URL <https://openreview.net/forum?id=Bkg6RiCqY7>.

Qing Lyu, Shreya Havaldar, Adam Stein, Li Zhang, Delip Rao, Eric Wong, Marianna Apidianaki, and Chris Callison-Burch. Faithful chain-of-thought reasoning. In *The 13th International Joint Conference on Natural Language Processing and the 3rd Conference of the Asia-Pacific Chapter of the Association for Computational Linguistics (IJCNLP-AACL 2023)*, 2023.

Aman Madaan, Niket Tandon, Prakhar Gupta, Skyler Hallinan, Luyu Gao, Sarah Wiegreffe, Uri Alon, Nouha Dziri, Shrimai Prabhumoye, Yiming Yang, et al. Self-refine: Iterative refinement with self-feedback. *Advances in Neural Information Processing Systems*, 36:46534–46594, 2023.

Andrea Montanari and Yiqiao Zhong. The interpolation phase transition in neural networks: Memorization and generalization under lazy training. *The Annals of Statistics*, 50(5):2816–2847, 2022.

Catherine Olsson, Nelson Elhage, Neel Nanda, Nicholas Joseph, Nova DasSarma, Tom Henighan, Ben Mann, Amanda Askell, Yuntao Bai, Anna Chen, et al. In-context learning and induction heads. *arXiv preprint arXiv:2209.11895*, 2022.

Alethea Power, Yuri Burda, Harri Edwards, Igor Babuschkin, and Vedant Misra. Grokking: Generalization beyond overfitting on small algorithmic datasets. *arXiv preprint arXiv:2201.02177*, 2022.

Noah Shinn, Federico Cassano, Ashwin Gopinath, Karthik Narasimhan, and Shunyu Yao. Reflexion: Language agents with verbal reinforcement learning. *Advances in Neural Information Processing Systems*, 36:8634–8652, 2023.

Parshin Shojaee, Iman Mirzadeh, Keivan Alizadeh, Maxwell Horton, Samy Bengio, and Mehrdad Farajtabar. The illusion of thinking: Understanding the strengths and limitations of reasoning models via the lens of problem complexity. *arXiv preprint arXiv:2506.06941*, 2025.

Jiajun Song, Zhuoyan Xu, and Yiqiao Zhong. Out-of-distribution generalization via composition: A lens through induction heads in transformers. *Proceedings of the National Academy of Sciences*, 122(6):e2417182122, 2025. doi: 10.1073/pnas.2417182122. URL <https://www.pnas.org/doi/abs/10.1073/pnas.2417182122>.

Daniel Soudry, Elad Hoffer, Mor Shpigel Nacson, Suriya Gunasekar, and Nathan Srebro. The implicit bias of gradient descent on separable data. *The Journal of Machine Learning Research*, 19(1):2822–2878, 2018.

Jianlin Su, Murtadha Ahmed, Yu Lu, Shengfeng Pan, Wen Bo, and Yunfeng Liu. Roformer: Enhanced transformer with rotary position embedding. *Neurocomputing*, 568:127063, 2024.

Miles Turpin, Julian Michael, Ethan Perez, and Samuel Bowman. Language models don't always say what they think: Unfaithful explanations in chain-of-thought prompting. *Advances in Neural Information Processing Systems*, 36:74952–74965, 2023.

Ashish Vaswani, Noam Shazeer, Niki Parmar, Jakob Uszkoreit, Llion Jones, Aidan N Gomez, Łukasz Kaiser, and Illia Polosukhin. Attention is all you need. *Advances in neural information processing systems*, 30, 2017.

Johannes Von Oswald, Eyvind Niklasson, Ettore Randazzo, João Sacramento, Alexander Mordvintsev, Andrey Zhmoginov, and Max Vladymyrov. Transformers learn in-context by gradient descent. In *International Conference on Machine Learning*, pages 35151–35174. PMLR, 2023.

Jason Wei, Yi Tay, Rishi Bommasani, Colin Raffel, Barret Zoph, Sebastian Borgeaud, Dani Yogatama, Maarten Bosma, Denny Zhou, Donald Metzler, et al. Emergent abilities of large language models. *Transactions on Machine Learning Research*, 2022a. ISSN 2835-8856.

Jason Wei, Xuezhi Wang, Dale Schuurmans, Maarten Bosma, Fei Xia, Ed Chi, Quoc V Le, Denny Zhou, et al. Chain-of-thought prompting elicits reasoning in large language models. *Advances in Neural Information Processing Systems*, 35:24824–24837, 2022b.

Yixuan Weng, Minjun Zhu, Fei Xia, Bin Li, Shizhu He, Shengping Liu, Bin Sun, Kang Liu, and Jun Zhao. Large language models are better reasoners with self-verification. In *Findings of the Association for Computational Linguistics: EMNLP 2023*, pages 2550–2575, 2023.

Xuandong Zhao, Zhewei Kang, Aosong Feng, Sergey Levine, and Dawn Song. Learning to reason without external rewards. *arXiv preprint arXiv:2505.19590*, 2025.

A Experimental details

Models. Our model follows the standard transformer architecture Vaswani et al. (2017) and the standard practice where layer normalization is placed before self-attention and feedforward neural network (FFN) Karpathy (2022). We also used RoPE Su et al. (2024) which is the default positional embedding for many LLMs. During training, we did not use any scheduler to adjust the learning rate.

- Number of layers (L): 3
- Number of heads (H): 2
- Model dimension: 128
- FFN dimension: 512
- Dropout: 0.01
- Theta parameter is RoPE: 10000
- Weight decay: 0.01

Training. Each training example follows the format in equation 1, consisting of 11 tokens plus an EOS token. We compute the autoregressive loss starting from the first \rightarrow token (the 6th token) through the final solution token. The two unfaithfulness metrics, along with auxiliary quantities such as prediction entropy, are computed online during training to avoid additional overhead. Training a single model under a given noise configuration—including all metric evaluations—takes approximately 50 minutes on a single NVIDIA A30 GPU.

B Additional experiment results

B.1 Validating simplicity bias: swapping prompt and reasoning

We investigate the effect of positional order on reasoning faithfulness, focusing on the noiseless setting for clarity. Specifically, we compare two configurations:

- No swap: $e_1 \rightarrow e_2 \rightarrow e_3$
- Swap: $e_2 \rightarrow e_1 \rightarrow e_3$

where (e_1, e_2, e_3) denotes a consistent reasoning chain. In addition to the original (no-swap) setting, we train a transformer on the swapped data using identical hyperparameters. After training, we compare the four faithfulness metrics, summarized in Table 2. For completeness, we restate the unfaithfulness metrics defined in the main text:

$$\begin{aligned} \text{RIR}_1 &:= \frac{\sum_{i \leq n} \mathbf{1}\{e'_{i,2} \neq e_{i,2}, e_{i,3} = e'_{i,3}\}}{\sum_{i \leq n} \mathbf{1}\{e'_{i,2} \neq e_{i,2}\}} \\ \text{RIR}_2 &:= \frac{\sum_{i \leq n} \mathbf{1}\{e'_{i,2} \neq e_{i,2}, e_{i,3} = e'_{i,3}\}}{\sum_{i \leq n} \mathbf{1}\{e'_{i,3} = e_{i,3}\}} \\ \text{IDS} &:= \frac{1}{n} \sum_{i=1}^n D_{\text{KL}}(\hat{f}_2(e_{i,1}, e'_{i,2}), \hat{f}_2(e_{i,1}, \tilde{e}_{i,2})) \\ \text{INR} &:= \frac{1}{n} \sum_{i=1}^n \mathbf{1}\left\{ \arg \max_{e \in \mathcal{V}_N} p(e \mid e_{i,1}, e'_{i,2}) = \arg \max_{e \in \mathcal{V}_N} p(e \mid e_{i,1}, \tilde{e}_{i,2}) \right\} \end{aligned}$$

For the swapped CoT format, we correspondingly redefine INR and IDS. Conceptually, both metrics are still defined via perturbations applied to e_2 ; however, after swapping, e_2 now appears in the first step of the

reasoning chain. Similarly, in the definitions of RIR_1 and RIR_2 , the functional roles of e_2 and e_3 remain unchanged, except that e_2 is now positioned at the beginning of the chain.

Table 2: Unfaithfulness metrics before and after swapping e_1 and e_2 on noise-free data.

DATA LAYOUT	RIR ₁	RIR ₂	IDS	INR
$e_1^0 \rightarrow e_2^0 \rightarrow e_3$	0	0	24.7	0
$e_2^0 \rightarrow e_1^0 \rightarrow e_3$	1.00	0.99	26.0	0

The intervention-based metrics (IDS and INR) remain nearly unchanged, indicating that the observed effect is not driven by positional order: the model inherently prefers to rely on the simpler e_2 for prediction. In contrast, both RIR scores drop from 1 in the original format to 0 after swapping, since relying on e_2 for prediction becomes a form of “skip-step” reasoning under the swapped ordering.

B.2 Reasoning phases

Further explanation for mixed reasoning mode. We hypothesize that, during training, the model enters a *mixed reasoning phase* in which its prediction behavior can be approximated as follows. Define the indicator

$$c(e_1, e_2) = \mathbf{1}\{f(e_1) = f_2(e_2)\},$$

and conjecture that the model effectively predicts according to

$$\hat{f}_2(e_1, e_2) \approx f_2(e_2) c(e_1, e_2) + U(1 - c(e_1, e_2)),$$

where U denotes the uniform distribution on \mathcal{V}_N . In other words, the model develops a form of self-verification: it compares the results computed from e_1 and e_2 , and whenever these results disagree, it outputs an approximately uniform predictive distribution.

To quantify this phenomenon, we consider the metric

$$\frac{1}{|\mathcal{I}|} \sum_{i \in \mathcal{I}} D_{\text{KL}}(\hat{f}_2(e_{i,1}, e'_{i,2}), U),$$

where U is the uniform distribution on \mathcal{V}_N , and

$$\mathcal{I} = \{i : f(e_{i,1}) \neq f_2(e_{i,2})\}$$

is the set of inconsistent chains. A smaller value of this metric indicates that, on inconsistent examples, the model’s predictive distribution is closer to uniform, providing stronger evidence that it has transitioned into the mixed reasoning (self-verification) phase.

Qualitative characteristics of phase diagrams. For noise levels $\varepsilon_1 = 0.01$ and $\varepsilon_1 = 0.1$, we construct phase diagrams with training compute on the x-axis and reasoning noise ε_2 on the y-axis. For each pair (compute, ε_2), we assign a phase according to which of three reference distributions—the stepwise solution, the skip-step solution, or a uniform distribution (evaluated only on inconsistent chains)—has the smallest KL divergence to the model’s predictive distribution.

As shown in Figure 9, we observe a clear qualitative pattern in phase development: as ε_2 increases, the model transitions from exhibiting two phases, to three, and eventually to four distinct phases. For larger values of ε_2 , increasing compute further drives a gradual shift from stepwise reasoning toward skip-step reasoning. Intuitively, a larger ε_2 (relative to ε_1) induces a greater gap in achievable prediction accuracy between different reasoning modes, and the model’s drive to maximize accuracy consequently pushes it toward adopting the skip-step reasoning strategy.

We also note that the model’s phase transitions and training dynamics are sensitive to both the training data and the optimization process. Figure 9 shows phase diagrams obtained by training the model on

three different training sets generated from the same underlying distribution but with different random seeds. Despite sharing the same data distribution, the resulting trajectories differ substantially across seeds, including the timing of each phase transition and even the final phase to which the model achieves.

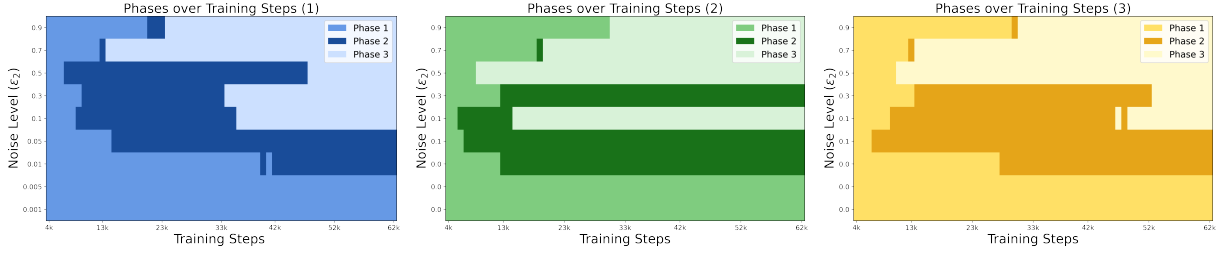


Figure 9: **Data quality and compute as deciding factors of reasoning modes.** We train models under fixed $\epsilon_1 = 0.1$ and varying ϵ_2 . More training steps (compute) and higher noise (data quality) tend to induce skip-step reasoning. The three panels show phase diagrams under three random seeds from the same data distribution, illustrating that the training dynamics are sensitive to randomness in the data and optimization.

Causal interpretations of three reasoning modes. Figure 10 illustrates three qualitatively distinct reasoning patterns. The first row depicts fully faithful stepwise reasoning, which is the ideal behavior we aim to elicit from the model during training. The second row shows a mixed reasoning mode: the model relies on e_1 when generating e_2 , and then uses both e_1 and e_2 when generating e_3 . This constitutes an unfaithful reasoning process, in which the model effectively couples e_2 and e_3 during inference. The third row presents another form of unfaithful reasoning, *skip-step deduction*, where the generation of e_3 depends solely on e_1 and is entirely independent of e_2 .

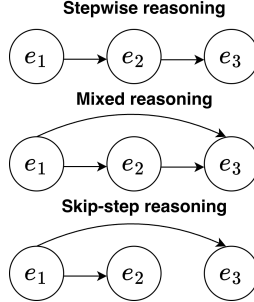


Figure 10: **Causal graphs representing three reasoning modes.** See Bao et al. (2024) for a similar causal perspective.

B.3 Additional results

Operator norm in Attention Contrast (AC). We briefly recall the notion of the matrix operator norm used in the definition of Attention Contrast (AC). Let $\|\cdot\|$ be a norm on \mathbb{R}^d . For a matrix $A \in \mathbb{R}^{d \times d}$, the (induced) operator norm of A with respect to $\|\cdot\|$ is defined as

$$\|A\|_{\text{op}} := \sup_{x \neq 0} \frac{\|Ax\|}{\|x\|} = \sup_{\|x\|=1} \|Ax\|.$$

Intuitively, $\|A\|_{\text{op}}$ measures the largest factor by which A can stretch a vector under the chosen norm. In the Euclidean case $\|\cdot\| = \|\cdot\|_2$, this coincides with the largest singular value of A , i.e., $\|A\|_{\text{op}} = \sigma_{\max}(A)$.

In our AC, the matrix inside the operator norm is

$$h_{L-1,i}^+ W_{QK}^{(L)} (h_{L-1,i}^+)^{\top} - h_{L-1,i}^- W_{QK}^{(L)} (h_{L-1,i}^-)^{\top},$$

which represents the difference between the last-layer attention score matrices for a positive (consistent) chain (e_1^+, e_2^+) and a negative (inconsistent) chain (e_1^-, e_2^-) at sample index i . The operator norm $\|h_{L-1,i}^+ W_{QK}^{(L)} (h_{L-1,i}^+)^T - h_{L-1,i}^- W_{QK}^{(L)} (h_{L-1,i}^-)^T\|_{\text{op}}$ thus captures the maximal change in attention scores along any direction in the representation space when we move from consistent to inconsistent chains. Averaging this quantity over i in the definition of AC yields a global measure of how strongly the model’s attention mechanism separates positive and negative samples, providing evidence for internal uncertainty encoding or self-verification behavior.

Phase 0 and format score. In Section 3.2, we hypothesize that there is an initial Phase 0 during training in which the model primarily learns the data format. Figure 11 shows how the format score evolves during training on datasets with noise levels $\varepsilon_1 = 0.01$ and $\varepsilon_2 = 0.1$. We observe that the format score rapidly increases from 0 to 1 within the first 1k steps, indicating that, in this early stage, model indeed first focuses on matching the data format. In Figure 11, we also plot how the model’s prediction accuracy evolves over training. In Phase 1, due to simplicity bias, the model first learns to perform stepwise prediction of e_3 from e_2 , achieving an accuracy of approximately $1 - p_2 = 90\%$. In P3, the model switches to skip-step reasoning, and the accuracy increases to about $1 - p_1 = 99\%$. In contrast, P2 is dominated by self-verification: according to our hypothesis, for samples with $f(e_1) = f_2(e_2)$ the model outputs an approximately uniform distribution and thus cannot predict the correct result. Consistent with this picture, the accuracy curve in Figure 9 does not increase during P2 but instead remains flat, providing indirect evidence for our proposed mechanism in Phase 2.

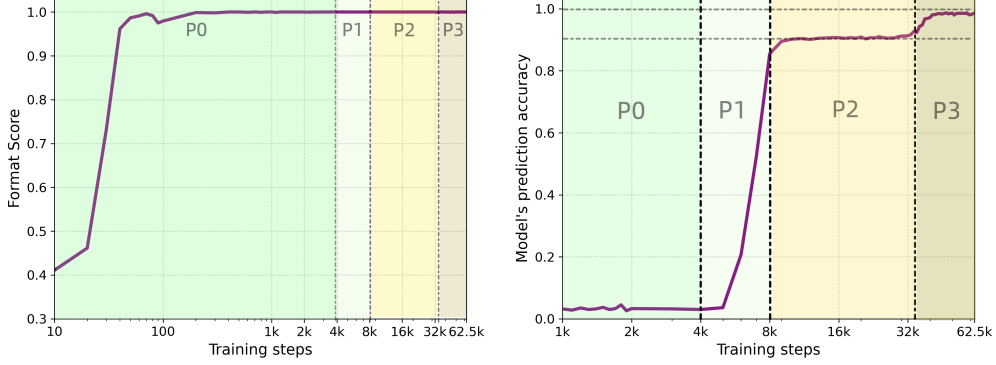


Figure 11: **Training trajectories of the model’s format score and predictive accuracy.** **Left: The format score over training steps.** During Phase 0, the model rapidly improves its accuracy in predicting the structural positions (operators and deduction tokens). **Right: The model’s prediction accuracy (on e_3) over training steps.** The model first learns to rely on e_2 and reaches an accuracy of about 90% in P1. In P2, the model develops a self-verification mechanism, which does not further improve prediction accuracy. Eventually, the model transitions to skip-step reasoning, and the accuracy increases to approximately 99%.

Additional unfaithfulness metrics. We present additional metrics for quantifying the model’s unfaithfulness. Figure 12 shows, over a grid of noise levels $\varepsilon_1 \in \{0.01, 0.1, 0.3, 0.5\}$ and $\varepsilon_2 \in \{0, 0.01, 0.1, 0.3, 0.5, 0.7\}$, the model’s consistency ratio (CR), interventional distribution sensitivity (IDS), and reasoning inconsistency ratio (RIR) after training. Since we compare RIR₂ across different values of ε_2 , we report a version of RIR₂ that is normalized by the effective noise level in ε_2 : Normalized RIR₂ = RIR₂ / ($n^{-1} \sum_{i \leq n} \mathbf{1}\{e'_{i,2} \neq e_{i,2}\}$). Figure 12 further shows that, for any fixed ε_1 , the model’s unfaithfulness increases as ε_2 grows. Moreover, as ε_1 becomes larger, the fraction of successful reasoning chains decreases, and the model increasingly favors stepwise reasoning over skip-step reasoning, as the latter no longer provides a meaningful improvement in prediction accuracy in this regime.

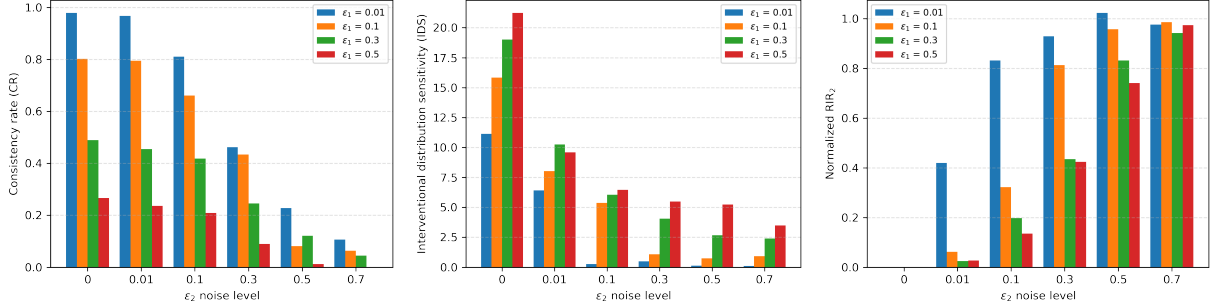


Figure 12: **Results of additional unfaithfulness metrics for models trained across different noise regimes.** **Left:** As ϵ_2 increases, the consistency ratio gradually decreases, indicating that the model becomes increasingly less capable of performing successful CoT reasoning. **Middle/Right:** IDS decreases with increasing ϵ_2 , whereas RIR_2 increases. Together, these trends corroborate that the model’s degree of unfaithfulness grows as the noise level becomes larger.

Further analysis of the optimization trajectory. During training, we also track the KL divergence between the model’s learned distribution and the corresponding theoretically optimal distribution: $p(e_3 | e_1, e_2)$, in order to better understand the optimization trajectory. Figure 13 shows the evolution of this KL divergence for the three noise configurations considered in the main text. For noise levels $(\epsilon_1, \epsilon_2) = (0.01, 0.1)$ and $(0.1, 0.01)$, the KL divergence eventually approaches zero, reflecting that the model converges to the respective optimal target distributions under these noise settings. In contrast, for $(\epsilon_1, \epsilon_2) = (0.1, 0.1)$, Figure 12 shows that within 62,500 training steps the model remains in Phase 2 (self-verification). From an optimization perspective, we hypothesize that this phase corresponds to a local minimum or saddle point in the loss landscape. When ϵ_1 and ϵ_2 are close, such critical structures appear more frequently, making it harder for the model to escape and thus requiring substantially more training steps.

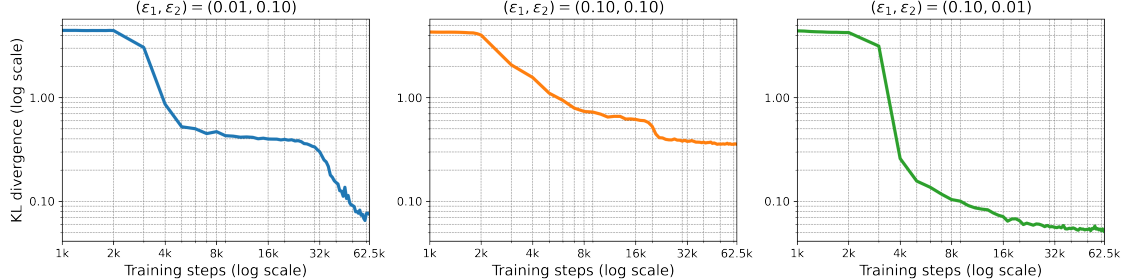


Figure 13: **KL divergence between the model’s learned distribution and the optimal distribution $p(e_3 | e_1, e_2)$ during training for three noise configurations.** For $(\epsilon_1, \epsilon_2) = (0.01, 0.1)$, the model converges to skip-step reasoning, and the KL divergence to the theoretical optimum goes to 0. Similarly, for $(\epsilon_1, \epsilon_2) = (0.1, 0.01)$, it converges to stepwise reasoning with vanishing KL. In contrast, for $(\epsilon_1, \epsilon_2) = (0.1, 0.1)$, the model gets stuck in the self-verification regime and does not reach the optimal predictive distribution.

B.4 Shortcut features

The left panel of Figure 14 shows the training-time trajectories of the consistency-based RIR_1 metric on the shortcut dataset and on the full dataset. A larger RIR_1 indicates more pronounced unfaithfulness on the corresponding data. We observe that throughout training, RIR_1 on the shortcut data remains consistently higher than the value computed on the full dataset, consistent with Figure 8. Notably, RIR_1 exhibits a step-like pattern over the course of training, whereas INR increases only once near the end of training. This difference arises because the definition of RIR_1 explicitly accounts for the model’s learning accuracy on e_2 ; as the model’s accuracy on e_2 improves steadily during training, RIR_1 increases in a corresponding stepwise manner.

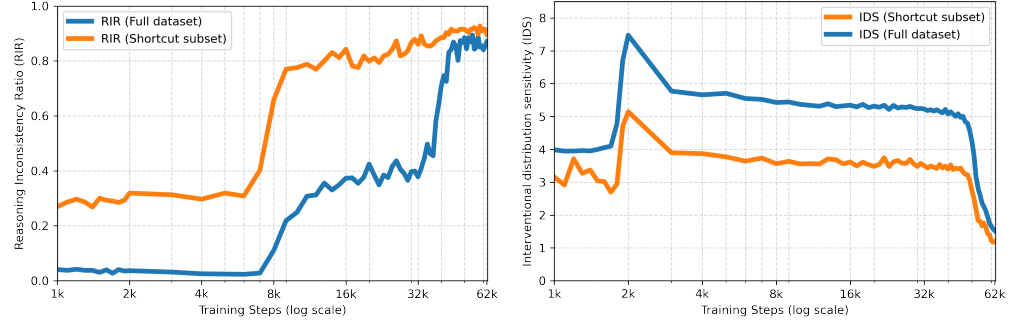


Figure 14: **Additional dynamics of unfaithfulness metrics on the shortcut and full datasets.** **Left:** Throughout training, the RIR_1 measured on the shortcut dataset remains consistently higher than that on the full dataset, indicating that the model is more unfaithful on shortcut data and likely exploits the shortcut. **Right:** Throughout training, the IDS on the shortcut dataset stays consistently lower than on the full dataset, suggesting reduced reliance on e_2 and a stronger tendency to adopt skip-step reasoning in the presence of shortcuts.

We plot the training trajectories of the metrics on the shortcut subset and the full dataset under different noise levels, as shown below.

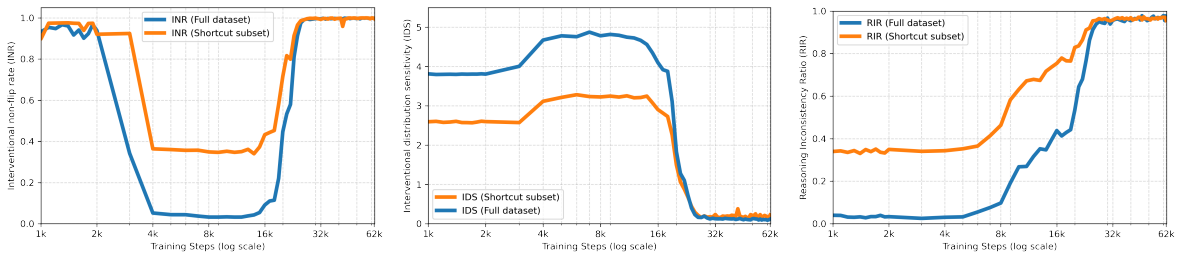


Figure 15: Training dynamics of INR, IDS, and RIR_1 under the setting $N = 94$ and noise configuration $(\varepsilon_1, \varepsilon_2) = (0.01, 0.3)$.

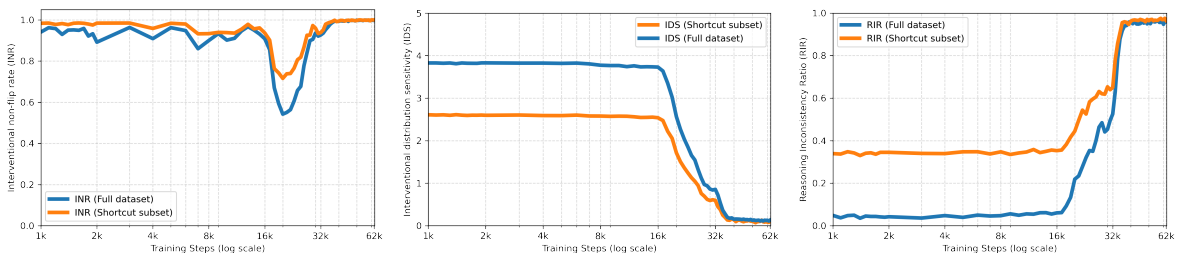


Figure 16: Training dynamics of INR, IDS, and RIR_1 under the setting $N = 94$ and noise configuration $(\varepsilon_1, \varepsilon_2) = (0.01, 0.5)$.

We repeat the experiments with the modulus reduced from 94 to 38 while fixing the noise levels to $(\varepsilon_1, \varepsilon_2) = (0.01, 0.1)$. The corresponding training metrics are shown in Figure 17.



Figure 17: Training dynamics of INR, IDS, and RIR₁ under the setting $N = 38$ and noise configuration $(\varepsilon_1, \varepsilon_2) = (0.01, 0.1)$.

C Ablations and variants of experiment setups

We present further results under variants of experimental setups.

Larger model size. We first fix the data setup (recall Eq. 1) and increase the model depth from 3 layers to 5 layers while keeping all other hyperparameters unchanged. Figure 18 compares the training dynamics of the 5-layer Transformer at noise level $(\varepsilon_1, \varepsilon_2) = (0.01, 0.1)$ with those of the 3-layer model, reporting the evolution of INR and the entropy of the model’s predictive distribution. The 5-layer model also eventually learns the skip-step reasoning strategy; however, its entropy curve becomes essentially monotone and no longer exhibits the non-monotonic “bump” associated with the Phase 2 self-verification regime. Consistently, the INR of the 5-layer model drops sharply and then quickly returns to 1 between 5k and 10k training steps, suggesting that the higher-capacity model spends little time in Phases 1 and 2 and rapidly transitions into the skip-step regime that achieves the optimal solution. In contrast, the 3-layer model lingers substantially longer in the stepwise and self-verification regimes, effectively getting trapped near these suboptimal local minima.

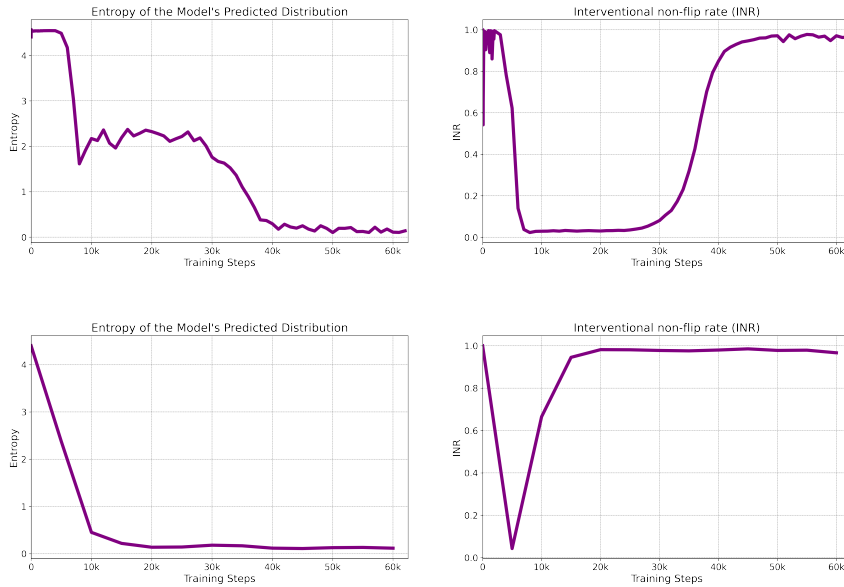


Figure 18: **Training dynamics of INR and entropy for 5-layer and 3-layer transformers.** The first row: INR and the entropy of the model’s predictive distribution over the course of training for the 3-layer transformer. The second row: The 5-layer transformer, owing to its larger capacity, rapidly acquires skip-step reasoning and passes through Phases 1 and 2 without a non-monotonic rise in entropy. This is reflected by the sharp transient fluctuations in INR early in training.

As capacity increases, the transition can become so rapid that intermediate phases are less visible. To better assess whether our qualitative phenomena persist at larger scales—i.e., whether they are *rescalable* rather than artifacts of a particular model or problem size—we further increase the task complexity by enlarging the modulus. Concretely, we increase the dataset modulus to $N = 113$ while keeping all other hyperparameters fixed, and train the same 5-layer Transformer under an identical experimental protocol. If the characteristic multi-phase dynamics re-emerge and remain qualitatively consistent in this larger-modulus regime, it provides evidence that our observations are robust to scaling in both model capacity and problem size.

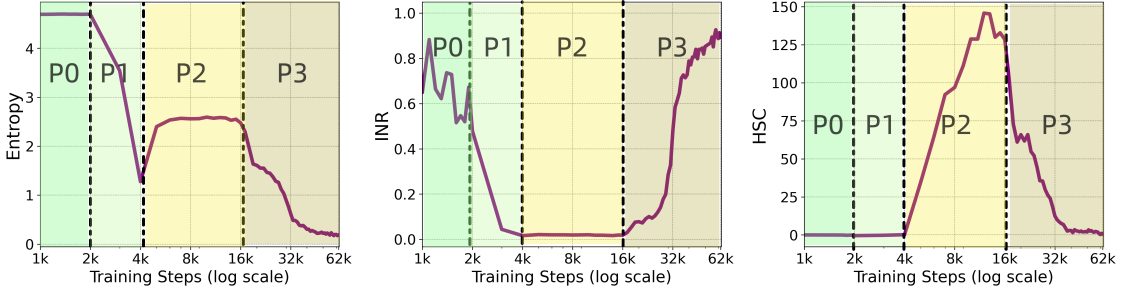


Figure 19: **Training dynamics of the 5-layer Transformer at noise levels $(\varepsilon_1, \varepsilon_2) = (0.01, 0.1)$ with modulus $N = 113$.** **Left:** In the 5-layer Transformer setting, the entropy of the model’s predictive distribution still clearly delineates the training process into four distinct phases. **Middle:** The INR metric computed for the 5-layer model captures the model’s transition across three reasoning modes, from stepwise to mixed and ultimately to skip-step reasoning. **Right:** During training, the 5-layer model also develops internal indicators that support self-verification, as evidenced by the corresponding evolution of the HSC.

Figure 19 summarizes the training trajectories of a 5-layer Transformer on the $N = 113$ setting with noise $(\varepsilon_1, \varepsilon_2) = (0.01, 0.1)$. We monitor the entropy of the model’s predictive distribution, an intervention-based unfaithfulness measure, and the HSC metric that quantifies self-verification behavior. Notably, even under this larger-modulus task and with increased depth, the learning process follows essentially the same qualitative pattern as in the 3-layer, $N = 97$ experiments. The model transitions from an initial stepwise regime, through an intermediate mixed regime, and ultimately converges to the skip-step strategy. The fact that these regime changes persist under simultaneous scaling of both model capacity and task size supports the view that the phenomena we observe reflect a robust, rescalable training dynamic rather than a peculiarity of a specific configuration.

Different modulus. We changed N from 97 to 83. Figure 20 and 21 show that for the modulus-83 setting, the training dynamics of the consistency-based and intervention-based unfaithfulness measures, as well as the model’s output entropy, prediction accuracy, and hidden state contrast (HSC). These metrics exhibit trends that closely mirror those observed under modulus 97, and the training process again shows clear phase transitions, with the model’s behavior in each phase remaining effectively the same as in the modulus-97 case.

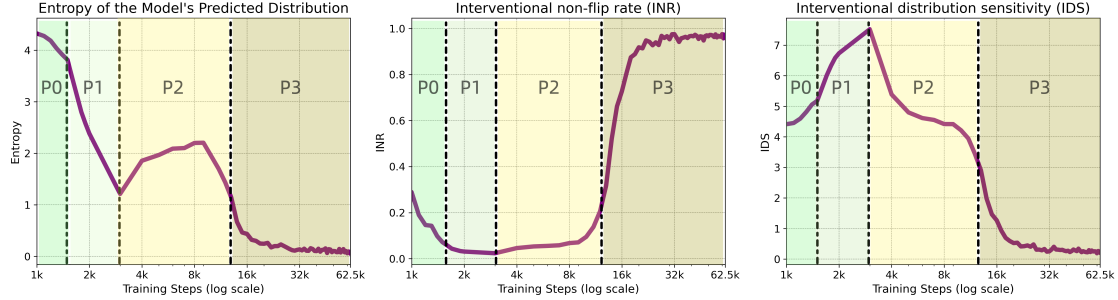


Figure 20: **Training dynamics at noise levels $(\varepsilon_1, \varepsilon_2) = (0.01, 0.1)$ with modulus $N = 83$.** **Left:** The entropy of the model’s output predictions. **Middle:** During training steps, INR first drops to zero, indicating that predictions of e_3 rely entirely on e_2 , and later rises toward one, showing that e_3 is eventually predicted solely from e_1 . **Right:** IDS first increases and then decreases, mirroring the change in the model’s reliance on e_2 .

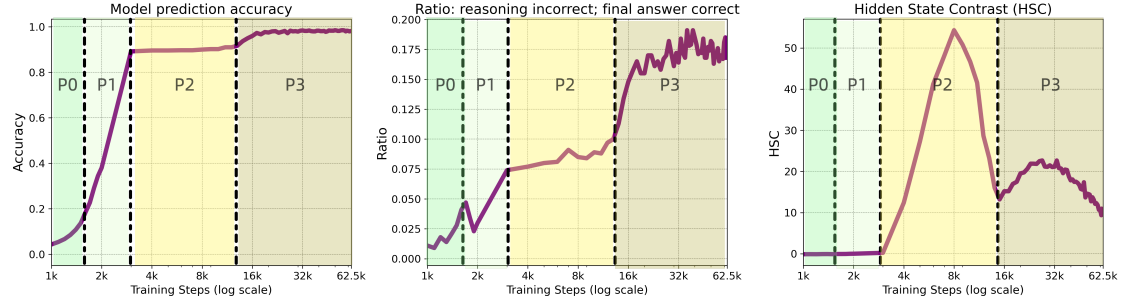


Figure 21: **Training dynamics at noise levels $(\varepsilon_1, \varepsilon_2) = (0.01, 0.1)$ with modulus $N = 83$.** **Left:** The model’s prediction accuracy reaches 90% in Phase 1, remains essentially unchanged throughout Phase 2, and then increases to around 99% in Phase 3, consistent with the evolution of the model’s internal reasoning mechanism. **Middle:** Unfaithfulness ratio: $e'_2 \neq e_2$, $e'_3 = e_3$. (Reasoning incorrect; final answer correct.) **Right:** Hidden state contrast (HSC) increases rapidly during Phase 2, but then drops sharply during the transition from Phase 2 to Phase 3, suggesting that a self-verification mechanism is forming within the model.

Figure 22 shows the trends of the model’s unfaithfulness metrics under four different noise levels: $\varepsilon_1 = (0.01, 0.1, 0.3, 0.5)$. As in the modulus-97 setting, for any fixed ε_1 the model retains a certain degree of stepwise reasoning below a critical threshold $\tau_c(\varepsilon_1)$; once ε_2 exceeds this threshold, the unfaithfulness measures increase sharply.

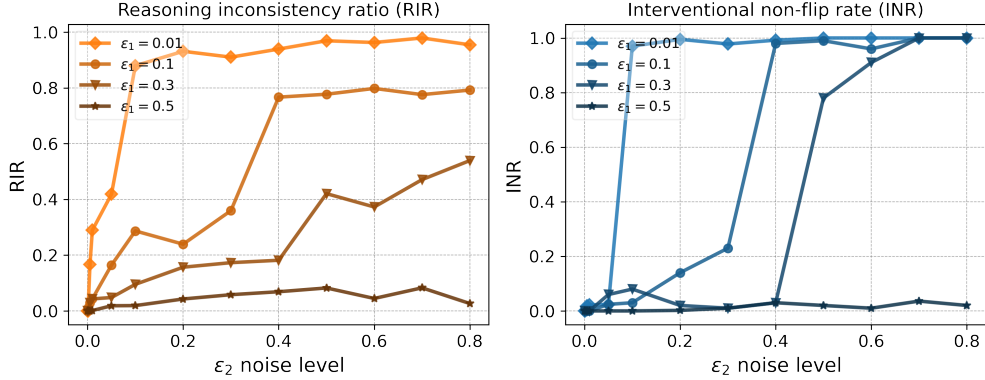


Figure 22: **Transformer models trained on modulus $N = 83$ datasets under varying noise levels.** For modulus 83, we evaluate CoT faithfulness under two definitions by training transformers on datasets with varying noise levels (ϵ_1 : prompt noise, ϵ_2 : reasoning noise). In the low-noise regime both unfaithfulness measures remain small, but beyond a critical ϵ_2 they increase sharply—orange curves indicate inconsistent reasoning chains, while blue curves show that interventions on the reasoning steps hardly affect the final answers.

Different data format. We consider an alternative training-example format in which parentheses are added to the prompt expression, while keeping the modulus consistent with the main text (i.e., $N = 97$). The modified data format is as follows:

$$\underbrace{(a \times b) - c}_{E_1:\text{prompt}} \rightarrow \underbrace{d - c}_{E_2:\text{reasoning}} \rightarrow \underbrace{e}_{E_3:\text{solution}}.$$

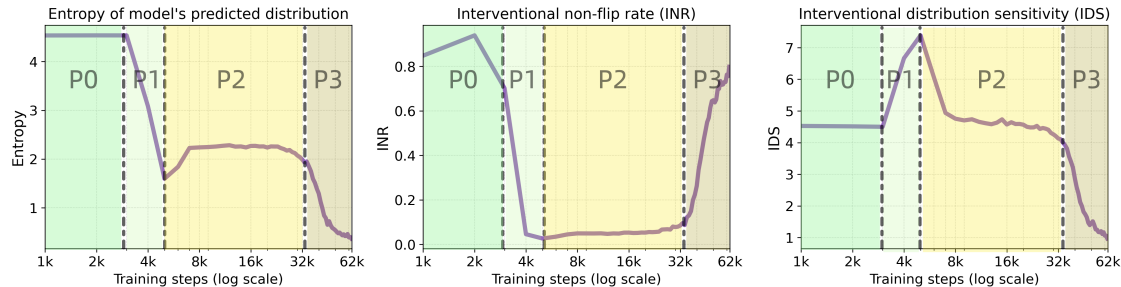


Figure 23: **Training dynamics on the parenthesized data variant.** **Left:** The entropy of the model’s output predictions. **Middle:** During training steps, INR first drops to zero, indicating that predictions of e_3 rely entirely on e_2 , and later rises toward one, showing that e_3 is eventually predicted solely from e_1 . **Right:** IDS first increases and then decreases, mirroring the change in the model’s reliance on e_2 .

Figure 23 shows the training dynamics on the parenthesized data variant. Overall, the model exhibits nearly identical behavior and phase transitions to those observed in the non-parenthesized setting. This is expected because parentheses in our construction merely standardize the surface form of the expressions and do not alter the underlying computation. Therefore, it is reasonable to focus on the simplest format—i.e., the version without parentheses (see Eq. 1)—for training and analysis.